JAMES | Journal of Advances in Modeling Earth Systems

RESEARCH ARTICLE
10.1029/2021MS002947

A One-Year-Long Evaluation of a Wind-Farm Parameterization in HARMONIE-AROME

Bart van Stratum[1,2], Natalie Theeuwes[1], Jan Barkmeijer[1], Bert van Ulft[1], and Ine Wijnant[1]

[1]Royal Netherlands Meteorological Institute (KNMI), de Bilt, The Netherlands, [2]Now at Department of Meteorology and Air Quality, Wageningen University, Wageningen, The Netherlands

Key Points:

- In this study a wind-farm parameterization is implemented in the numerical weather prediction model HARMONIE-AROME
- A model evaluation of a full year reveals the wind-farm parameterization improves wind-speed forecasts close to offshore wind farms
- The presence of wind farms in the model also alters temperature and humidity profiles due to the enhanced turbulent mixing by the turbines

Supporting Information:

Supporting Information may be found in the online version of this article.

Correspondence to:

N. Theeuwes,
natalie.theeuwes@knmi.nl

Citation:

van Stratum, B., Theeuwes, N., Barkmeijer, J., van Ulft, B., & Wijnant, I. (2022). A one-year-long evaluation of a wind-farm parameterization in HARMONIE-AROME. *Journal of Advances in Modeling Earth Systems*, *14*, e2021MS002947. https://doi.org/10.1029/2021MS002947

Received 10 DEC 2021
Accepted 23 JUN 2022

Abstract The need to mitigate climate change will boost the demand for renewable energy and lead to more wind turbines both on- and offshore. In the near future, the effect these wind farms have on the atmosphere can no longer be neglected. In numerical weather prediction models wind-farm parameterisations (WFP) can be used to model the effect of wind farms on the atmosphere. There are different modeling approaches, but the parameterization developed by Fitch et al. (2012) is mostly used in previous studies. It models the wind farm as a momentum sink and a source of power production and turbulent kinetic energy. In this paper, we have implemented the Fitch et al. (2012) WFP into HARMONIE-AROME, the numerical weather prediction model that is currently used by at least 11 national weather services in Europe. We used HARMONIE-AROME to make year-long simulations for 2016 with and without the WFP. The results were extensively evaluated using lidar, tower and flight measurements at several locations near wind farms. Including the WFP reduces the model bias for wind speed near offshore wind farms. Wind farms not only affect wind, but also temperature and humidity, especially during stable atmospheric conditions: the enhanced mixing caused by the wind turbines reduces the stratification of temperature and humidity. Including the WFP in HARMONIE-AROME results in a more realistic representation of the atmosphere near wind farms and makes it a more future-proof model for weather forecasting.

Plain Language Summary Wind power production is steadily increasing. Wind farms are growing both in number and size, while weather models evolve to higher resolutions. This means that the effect of wind farms can no longer be ignored by weather prediction models. Wind farms essentially decelerate the wind (blockage and wake effects) and increase turbulence, indirectly influencing temperature and humidity. In this study, we have included a widely used wind-farm parameterization in the operational weather prediction model. The model is evaluated using various datasets, for example, power production data, flight and floating lidar measurements, and anemometer measurements from a tower. The inclusion of the wind-farm parameterization improves the wind forecasts near wind farms, also improving the estimate in power production. In addition, we are able to model the effects of wind farms on the near-surface temperature and humidity.

1. Introduction

Offshore wind power production in the European Union (EU) and specifically the North-Sea region is steadily increasing: the Dutch offshore capacity is expected to grow from ~1 GW in 2019 to ~11.5 GW in 2030, as part of a total expected increase to ~70 GW in the entire EU (WindEurope, 2017). Wind turbines produce electric energy by extracting kinetic energy from the atmosphere, thereby decelerating (and mixing) the air. This typically results in a downstream decrease in wind speed and increase in turbulence (e.g., Baidya Roy & Traiteur, 2010; Fitch et al., 2012). As wind farms grow—Both in size and number—The impact on weather and climate is expected to become more significant, requiring an adaptation of mesoscale models like HARMONIE-AROME (hereafter: HARMONIE) to account for the influence of wind farms on the local and regional meteorological conditions.

There are several ways in which the effects of wind turbines on the atmosphere can be parameterized in mesoscale models (Fischereit et al., 2021): Implicit—Imposing an additional roughness to implicitly model the effect of wind turbines on the atmospheric flow—Or explicit, explicitly solving the momentum sink and enhanced turbulence production due to the presence of wind turbines. In the last two decades several explicit parameterisations have been developed (e.g., Abkar & Porté-Agel, 2015; Fitch et al., 2012; Volker et al., 2015). The most commonly used and evaluated parameterization is the Fitch et al. (2012) model implemented in the Weather Research and Forecasting (WRF) model (Skamarock et al., 2019).

In this study, we implemented the wind turbine parameterization from Fitch et al. (2012) in HARMONIE. Where wind turbines are located, this parameterization adds an elevated drag term to the atmosphere, which locally decelerates the flow. The kinetic energy that is extracted from the atmosphere, but not converted into electric power, is used as a source term for turbulent kinetic energy (TKE).

HARMONIE with the newly-implemented wind-farm parameterization is evaluated using doppler lidar and tower measurements over the North Sea and compared to HARMONIE without wind-farm parameterization. This is done for one full year (January up to and including December 2016), instead of short case studies as is done in most evaluations of wind-farm parameterisations (e.g., Lee & Lundquist, 2017; Wu et al., 2022). The parameterization is evaluated for all seasons with varying wind directions and atmospheric stabilities. In 2016, measurements were available from two floating lidars in the Borssele wind farm zone (in the North Sea, off the Belgian coast), one ground-based lidar in the Westermost Rough wind farm (off the east coast of the UK), cup-anemometer measurements on the FINO1 tower near the Alpha Ventus wind farm in the North Sea (north of the Netherlands) and aircraft measurements (off the northwest German coast). Since all these measurements are in or near existing wind farms, they are ideal for evaluating the newly implemented wind-farm parameterization. The spatial impact of the wind farms on the wind fields is evaluated using dedicated flight campaigns (Lampert et al., 2020). The consequence of the WFP on power production is evaluated using Belgian transmission system operator (TSO) data. Moreover, the year-long experiment allowed us to quantify the impact of the offshore wind farms on the offshore and coastal meteorological conditions.

2. Model Description and Set-Up

The wind-farm parameterization is implemented in HARMONIE-AROME (cycle 40h1), a non-hydrostatic model developed by the HIRLAM-C consortium, which is operationally used in at least 11 countries (Bengtsson et al., 2017). The model uses a semi-Lagrangian scheme on an Eulerian grid. The HARATU turbulence scheme (de Rooy et al., 2022; Lenderink & Holtslag, 2004) was used, which uses a prognostic equation for the turbulent kinetic energy (TKE). Shallow convection follows de Rooy et al. (2022). Surface Externalisée (SURFEX) version 7.3 was used as a land surface model (Masson et al., 2013) with the land use classification from ECOCLIMAP II (Faroux et al., 2013). More details about the model physics can be found in Bengtsson et al. (2017) or www.hirlam.org.

For the simulations, HARMONIE used a 2000×2000 km^2 domain with 65 vertical levels, a 2.5 km horizontal grid spacing (which is currently the operational HARMONIE resolution at the Royal Netherlands Meteorological Institute (KNMI)), centered around 51.96°N, 4.9°E, and the ERA5 reanalysis (Hersbach et al., 2020) for the lateral boundary conditions and sea surface temperature. The lateral boundary conditions are updated hourly and coupled using the Davies–Kallberg relaxation scheme (Davies, 1976). The sea surface temperature in ERA5 only changes once every 24 hr.

Two simulations were performed: (a) reference simulation without wind turbines, REF, and (b) with the wind-farm parameterization, modeling all offshore wind turbines in the model domain in January 2016, WFP. The experiments are run from 01 to 01-2016 00 UTC to 01-01-2017 00 UTC. This period was chosen because of the availability of two floating lidars in the Borssele wind farm zone, directly north-east of the (Belgian) Northwind wind farm (Figure 2). In addition, there are tower measurements from the FINO1 platform, and lidar measurements from the Westermost Rough wind farm and flights through wind farm wakes in the German Bight (WIPAFF; Lampert et al., 2020) for this period.

The reference simulation was run for several years before the study period for the Dutch Offshore Wind Atlas (DOWA) project (Wijnant et al., 2019) and therefore had more than 1 year of spin-up. The WFP run was started "warm" from the control experiment and had 10 days of additional spin-up time. Both reanalysis simulations used 3D-VAR data assimilation (Fischer et al., 2005; Gustafsson et al., 2018) with a three-hour cycling time. In addition to conventional observations, Mode-S EHS aircraft measurements (e.g., de Haan, 2011; de Haan, 2016) and Scatterometer (ASCAT) (Marseille & Stoffelen, 2017) were assimilated. In this study the 3-hr forecast is used as a proxy for the analysis.

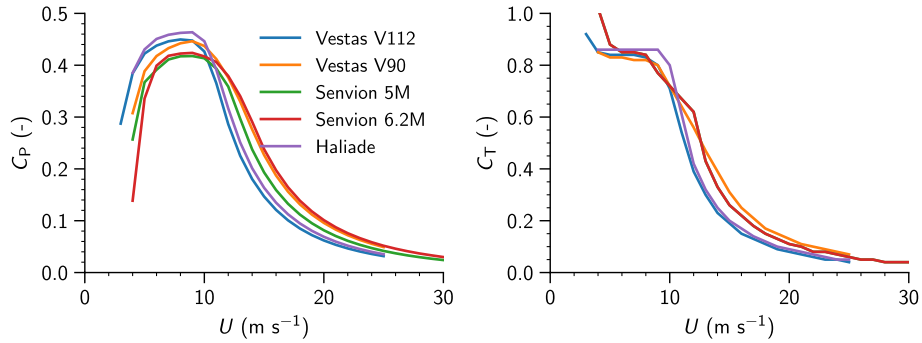

Figure 1. Power (C_P) and thrust (C_T) coefficients of the Belgian offshore wind turbines.

3. Wind-Farm Parameterization

The wind-farm parameterization of (Fitch et al., 2012) imposes an elevated momentum sink on the mean flow, where the drag (or thrust) of the individual turbine blades is modeled as a wind speed dependent drag force across the area swept by the rotor blades. As the diameter of a wind turbine is about an order of magnitude smaller than the horizontal grid spacing in HARMONIE (currently: 2.5 km), the model accounts for the bulk influence of one or several wind turbines per grid point.

The wind turbine characteristics are defined by the geometry (hub-height z_{hub} and turbine radius r), the cut-in (V_{in}) and cut-out (V_{out}) wind speeds, and by the dimensionless power (C_{P}) and thrust (C_{T}) coefficients. The latter two describe—As a function of wind speed V_{hub} at hub height—The fraction of kinetic energy that is extracted from the air (C_{T}), and the fraction that is converted into electrical energy (C_{P}). An example of typical C_{P} and C_{T} curves is provided in Figure 1.

Given the thrust coefficient C_{T} as a function of the absolute wind speed $|\vec{V}|$, the thrust force of a turbine (the force opposite to the flow direction and drag force) is defined as:

$$\vec{F}_{\text{thrust}} = -\frac{1}{2}\rho C_{\text{T}}|\vec{V}|\vec{V}A_T \tag{1}$$

where ρ is the air density (kg m^{-3}), $\vec{V} = (u, v)$ the horizontal wind vector (m s^{-1}), $|\vec{V}| = \sqrt{u^2 + v^2}$, and A_T is the rotor area (m^2). The rate of loss of kinetic energy (KE) then equals:

$$\left.\frac{\partial \text{KE}}{\partial t}\right|_{\text{drag}} = -\frac{1}{2}\rho C_{\text{T}}|\vec{V}|^3 A_T. \tag{2}$$

In practise the rotor of a turbine intersects multiple model levels, and Equation 2 (and all equations in the remainder of this chapter) are solved for each model level k individually, replacing the rotor area A_T with the area intersected by the k-th model level, and the wind speed $|\vec{V}|$, and density ρ with values from the k-th model level, indicated where appropriate by a subscript k. As a result, the momentum sink (and TKE source) is elevated and height dependent.

In general, the total change in KE imposed by a single wind turbine on a single grid cell with a volume $\Delta_k = (\Delta x \Delta y \Delta z_k)$ m^3 equals:

$$\left.\frac{\partial \text{KE}_{\text{k}}}{\partial t}\right|_{\text{cell}} = \frac{\partial}{\partial t}\left(\frac{1}{2}\rho_k|\vec{V}_k|^2\right)\Delta_k = \rho_k|\vec{V}_k|\frac{\partial|\vec{V}_k|}{\partial t}\Delta_k. \tag{3}$$

Combining Equations 2 and 3, that is, setting:

$$\left.\frac{\partial \text{KE}_{\text{k}}}{\partial t}\right|_{\text{cell}} = \left.\frac{\partial \text{KE}_{\text{k}}}{\partial t}\right|_{\text{drag}}, \tag{4}$$

results, after re-arranging, in an expression for the change in velocity with time:

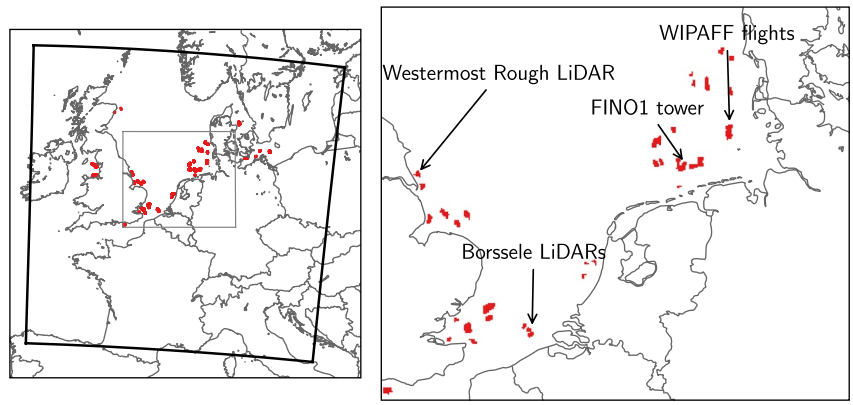

Figure 2. Overview of all (2.5 × 2.5 km) grid points with one or more wind turbines (red). Black arrows indicate the locations of measurements used for evaluation. In the left figure the black square indicates the model domain and the gray square the location of the right panel.

$$\frac{\partial|\vec{V}_k|}{\partial t} = -\frac{1}{2} C_{\mathrm{T}} \; |\vec{V}_k|^2 \; A_k \; \Delta_k^{-1}, \tag{5}$$

or, in component form:

$$\frac{\partial u_k}{\partial t} = -\frac{1}{2} C_{\mathrm{T}} \; u_k \; |\vec{V}_k| \; A_k \; \Delta_k^{-1}, \tag{6}$$

$$\frac{\partial v_k}{\partial t} = -\frac{1}{2} C_{\mathrm{T}} \; v_k \; |\vec{V}_k| \; A_k \; \Delta_k^{-1}. \tag{7}$$

The vertical velocity component is assumed to be unaffected by the wind turbines, and furthermore, drag by the wind turbine tower and nacelle is not included in the parameterization. The energy that is extracted from the atmosphere, but not converted into electrical energy, is assumed to be converted into turbulent kinetic energy (TKE, per unit mass), that is, $C_{\mathrm{TKE}} = C_{\mathrm{T}} - C_{\mathrm{P}}$, resulting in:

$$\frac{\partial \mathrm{TKE_k}}{\partial t} = \frac{1}{2} C_{\mathrm{TKE}} \; |\vec{V}_k|^3 \; A_k \; \Delta_k^{-1}. \tag{8}$$

We should note that our choice for $C_{\mathrm{TKE}} = C_{\mathrm{T}} - C_{\mathrm{P}}$—In line with (Fitch et al., 2012)—Is somewhat arbitrary. For example, (Archer et al., 2020) suggest reducing C_{P} to 25% of its original value, while others (e.g., Siedersleben et al., 2020) concluded that the original definition of C_{TKE} performed satisfactorily when comparing the resulting TKE with observations.

Finally, as a diagnostic quantity, the model outputs the electrical power produced by the wind turbines:

$$\mathrm{P} = \frac{1}{2} \rho C_{\mathrm{P}} \; A_T \; |\vec{V}_{\mathrm{hub}}|^3. \tag{9}$$

For a typical offshore wind farm, multiple wind turbines can occupy a single horizontal grid point. Instead of introducing a horizontal wind turbine density—Like in (Fitch et al., 2012)—Equations 6–9 are repeated for each individual turbine, allowing different turbine types in a single horizontal grid point. The total tendencies for the horizontal wind components and TKE are adjusted after the turbulence scheme is called and fed back to the model.

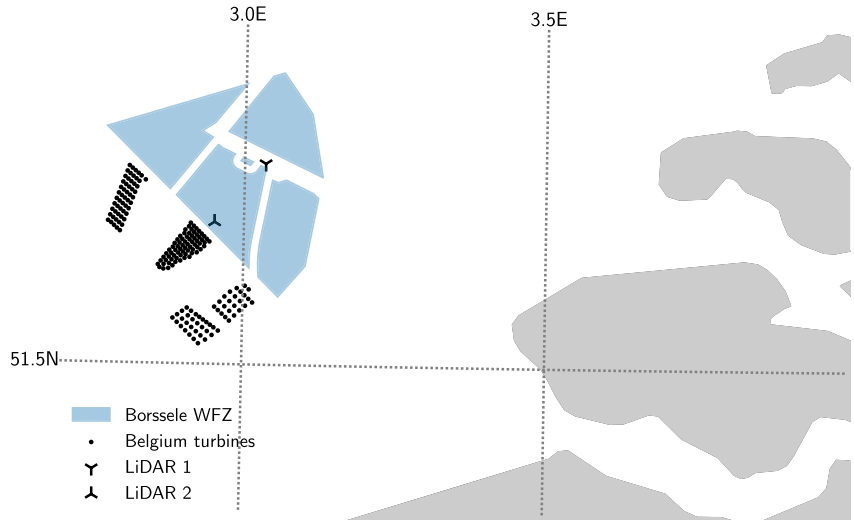

Figure 3. Setup of the Borssele wind lidars off the coast of Belgian and the Netherlands. The blue area are the planned wind farm zones, that started to be operational in 2020/2021.

4. Setup of Wind Turbines in the Domain

In the HARMONIE-AROME domain 3908 wind turbines with 18 different types are included (Figure 2). For the Belgian and Dutch wind farms, the exact (individual) turbine coordinates are available, which could directly be used in the experiments. For the other offshore wind farms in the computational domain (Figure 2), the available information was limited to the wind farm boundaries and the total number of turbines per wind farm. For these sites, the turbine coordinates were first chosen randomly within the wind farm boundary, and next distributed uniformly using an iterative repulsion method (Witkin & Heckbert, 2005). This random approach to determine the turbine coordinates can be justified by the fact that within the turbine parameterization, all turbines are mapped to the nearest 2.5×2.5 km grid point, making the exact turbine coordinates less important. The wind farm boundaries were obtained from the *The European Marine Observation and Data Network* (EMODnet; Martín Míguez et al., 2019).

The C_P and C_T curves were obtained from various sources, predominantly from windPRO input database (Acker & Chime, 2011). For a small number of turbines, no C_P and C_T curves were publicly available, those turbines have been replaced with either reference data from literature, or C_P and C_T curves from similar turbines. An overview of the wind farms and the turbine types is provided in the supplementary information.

5. Measurements

5.1. Borssele Wind Lidars

For the wind resource assessment of the four wind farms in the Borssele wind farm zone (BWFZ), two short-range doppler lidars were deployed near the Belgian offshore wind farms. Fugro executed a Metocean campaign and did measurements for a number of periods between June 2015 and February 2017. ZephIR 300S lidars were mounted on buoys with a bottom mooring weight at 51.707°N, 3.035°E (Figure 3, lidar 1) and at 51.646°N, 2.951°E (Figure 3, lidar 2). Lidar 1 (henceforth BWFZ1) measured for the longest period and there were 16 measurement periods between June 2015 and February 2017 (Figure 4a). This lidar is located 10 km northeast of the nearest wind turbine. Lidar 2 (henceforth BWFZ2) only measured during five periods and only between February and July 2016 (Figure 4b). This lidar is closer to the Belgian wind farm zones, at 2 km from the nearest turbine (Figure 3). At typical hub heights of about 90 m the uncertainty in floating lidar measurements for wind speeds between 4 and 15 m/s is between 3% and 4.5% (Duncan et al., 2019).

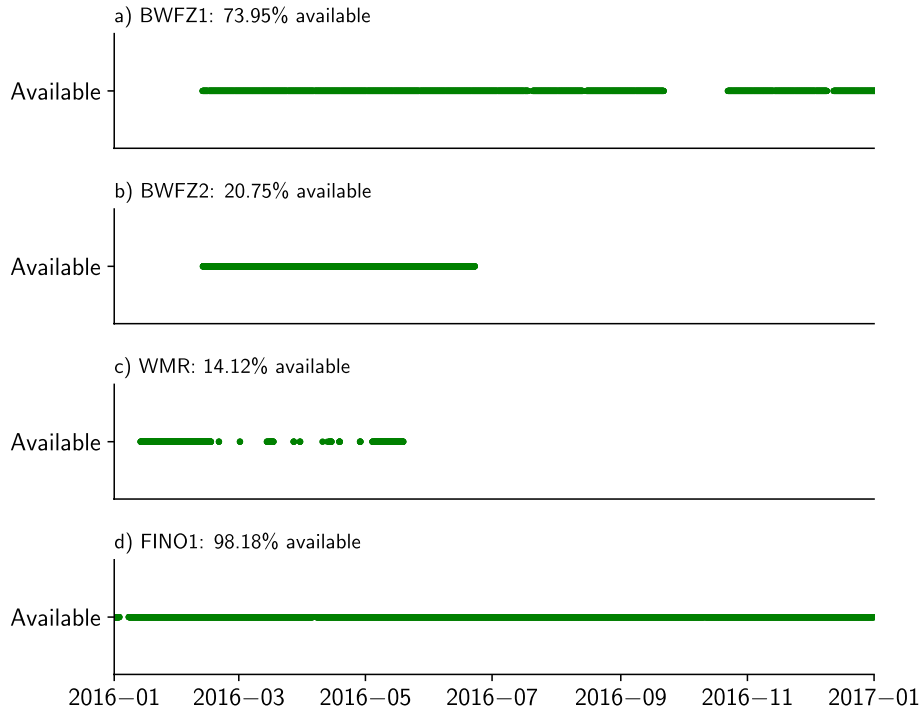

Figure 4. Availability of the measurements for the two lidars at the Borssele wind farm zone (a) BWFZ1 and (b) BWFZ2, (c) the Westermost Rough lidar (WMR) and (d) FINO 1.

5.2. FINO 1 Tower

The FINO 1 tower has been providing measurements since 2003 and is located in the North Sea at 54.015°N, 6.588°E, 50 km north of the Wadden island Borkum (Figure 2). The water depth at this location is 30 m and the tower reaches a height of 103.7 m above Lowest Astronomical Tide (LAT). The first wind turbines were installed near FINO1 in November 2009 and the Alpha Ventus wind farm became fully operational in 2010. This means that wind measurements for wind directions between 15° and 165° (easterly winds) became disturbed by Alpha Ventus since November 2009. Borkum Riffgrund 1 to the south west has been fully operational since 2015, also disturbing the flow in 170°–300° directions.

Here, we use the cup anemometers to evaluate the model, since these measure at frequent height intervals (i.e., 34.1, 41.6, 51.6, 61.6, 71.6, 81.6, 91.6, 101.6). The cup anemometers are manufactured Vector Instruments Windspeed Ltd. type A100LK/PC3/WR with an accuracy of 1%. The cup anemometers (for measuring wind speed) are on booms on the southeast side of the mast (toward 135–143°) and the wind vanes (for measuring wind direction) on booms on the opposite side of the mast. The wind speed measurements are corrected for wind mast effects using a measurement correction scheme called the UAM-correction method (i.e., Westerhellweg et al., 2010, 2012). Wind direction measurements are not corrected.

The FINO1 measurements are available for the whole of 2016 and only about 2.5% of the data are missing (Figure 4). Due to its long-term measurements the tower has been previously used to evaluate atmospheric models over the North Sea (e.g., Muñoz-Esparza et al., 2012; Wagner et al., 2019).

5.3. Westermost Rough Wind Lidar

On top of the Westermost Rough wind farm substation (Figure 2), Ørsted operates a Leosphere WindCube scanning doppler lidar, providing wind speed measurements between 74 and 324 m height. Westermost Rough wind farm is located off the coast of Yorkshire, UK. Unlike the Borssele lidars and FINO1 tower, this lidar is located in the center of the wind farm (53.804°N, 0.132°N), and is therefore always disturbed by the wind turbines. The Westermost Rough (WMR) lidar became operational in mid-January 2016, but only has an overall availability of ∼14% (1.5 out of 12 months), which limits its usability.

5.4. WIPAFF

As part of the WInd PArk Far Field (WIPAFF) project (Platis et al., 2020), several measurements were taken around wind farms in the German Bight area (Figure 2). In total 41 flights were carried out, of which 8 were in our current study period (6–10 September 2016). The aircraft measurements were carried out using the research aircraft Dornier 128. The aircraft is equiped with sensors measuring temperature, humidity, all wind components, and pressure at 100 Hz. This large data set of spatial data is very valuable to evaluate mesoscale models with wind-farm parameterisations, and has been used previously to evaluate the Weather Research Forecasting model (WRF) (Platis et al., 2021; Siedersleben et al., 2020; Siedersleben, Lundquist, et al., 2018; Siedersleben, Platis, et al., 2018). The measurements are described in detail by Lampert et al. (2020) and data are publicly available (Bärfuss et al., 2019).

For the purpose of this study we have only used one of the flights to evaluate the spatial representation of the wind farm wakes generated by HARMONIE. This flight took place on 6 September 2016, between 12:13 and 15:20 downwind of Amrumbank West wind farm. During this day the average background wind speed was about 7 m s^{-1} from the south according to Lampert et al. (2020). Therefore the aircraft measurements were taken in a meandering pattern north of the wind farm at hub height (i.e., 90 m). Given the average speed of the airplane was 54 m s^{-1} and to compare with the model data at a grid spacing of 2.5 km, a 60-s rolling average over the sonic anemometer data is performed.

5.5. Power Production Data

Belgium's high-voltage TSO, Elia, publishes the generated power by their various energy sources, including offshore wind farm power production in 15-min intervals. Since in 2016 Belgium only had three offshore wind farms (Figures 2 and 3), we are able to use their power generation data to evaluate the HARMONIE-modeled generated power. The total capacity of these offshore wind farms was 712.2 MW.

6. Evaluation

6.1. Offshore Lidar and Tower Measurements

During the chosen period, all lidars had periods with missing data, as summarized in Figure 4. For all statistical analyses in this section we use collocated data, that is, missing data is removed (or masked) in the model data set as well. In addition, there is no conditional sampling based on (e.g.,) wind direction; all available measurements are always included in the statistics.

6.1.1. Borssele Wind Farm Zone (BWFZ) Lidars

As shown in Figure 3, both lidars were positioned north-east of the Belgian Northwind wind farm. With prevailing winds from the south-west, these lidar measurements are typically disturbed by the Belgian wind farms, making them ideal for assessing the impact of the wind turbines on the wind field, and the ability of the wind farm parametrization to reproduce the disturbed wind field due to the wake effect of the wind farm.

Figure 5 shows the time averaged vertical wind speed profiles from the reference run (REF), the experiment with the wind-farm parameterization (WFP), and the Borssele lidars. These are averaged profiles over the entire measurement period for both lidars and represent all different wind directions. However, over the duration of the measurement period of BWFZ1, the wind direction was southwesterly (180–270°) 42% of the time.

For both sites the reference simulation (without wind park parameterization) overestimates the wind speed, which is most pronounced for lidar location number two, which is closest to the Belgian wind farms at 2 km distance from the nearest turbine. Enabling the wind-farm parameterization clearly improves the experiments; for BWFZ2, the mean profile from HARMONIE matches very well with the measurements.

6.1.2. FINO1 Tower

The FINO1 tower is situated directly west of the Alpha Ventus wind farm, and north-east of the Borkum Riffgrund wind farm (Figure 2). Figure 6a shows the time averaged vertical wind speed profiles, compared to the corrected FINO1 measurements. In line with the results from the Borssele area, the reference simulation overestimates the wind speed with ∼0.76–0.94 m s^{-1} (Table S5 in Supporting Information S1). With the wind-farm

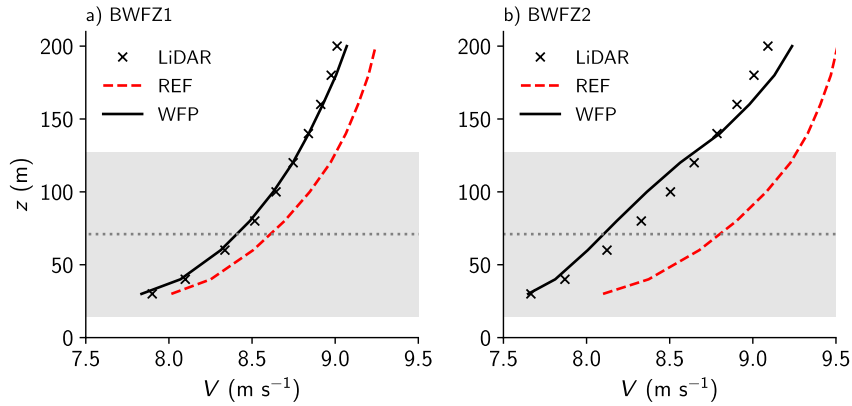

Figure 5. Vertical profiles of wind speed, from the reference run (REF) and experiment with wind-farm parameterization (WFP), compared to the Borssele (a) Borssele wind farm zone (BWFZ) lidar 1, 10 km from the nearest wind farm and (b) BWFZ lidar 2, 2 km from the nearest wind farm. The gray dotted line indicates the mean hub height of the nearest wind farm and the gray shaded areas the area the diameter of the rotor.

parameterization included, the absolute bias is decreased, but with a slight negative bias at the highest few measurement points, ∼0.04–0.21 m s^{-1} (Table S5 in Supporting Information S1). This underestimation seems to be partially caused by the mapping of wind turbines to the nearest HARMONIE grid point. In reality, the FINO1 tower is west (and with the dominating wind direction: upstream) of the Alpha Ventus wind farm, but in HARMONIE the grid point nearest to FINO1 also houses some of the Alpha Ventus wind turbines, as shown in Figure 6b. This means that the grid point used for the analysis, directly experiences drag from some of the Alpha Ventus turbines, resulting in a reduced wind speed. However, including the wind-farm parameterization clearly improves the wind profile at the tower location due to the many wind farms in the surroundings. This is also the location where the largest impact is expected.

The long measurement period of FINO1 allows us to make a more detailed comparison and verify the model simulations based on wind direction (Figure 7). The mean bias and root mean squared errors close to hub height (81 m), show a significant improvement across all wind directions between 20 and 330°, especially those which include the most wind turbines, between 80 and 110° and 160 and 240°. As also seen in Figure 6 the mean bias in the WFP run, is generally negative especially from the southern wind directions (minimum mean bias: −0.98 m s^{-1} around 170°). This means that either the background wind is underestimated, or the velocity deficit is overestimated by (Fitch et al., 2012) wind farm parameterization. This negative bias for wind directions influenced by wind farm is not as clear when examining the data from the BWFZ lidars (Supporting Information S1). In addition, in Section 6.2, we will examine the size and strength of the wake using flight measurements. The correlation coefficients are very similar between the experiments. This is as expected given the nature of the wind-farm

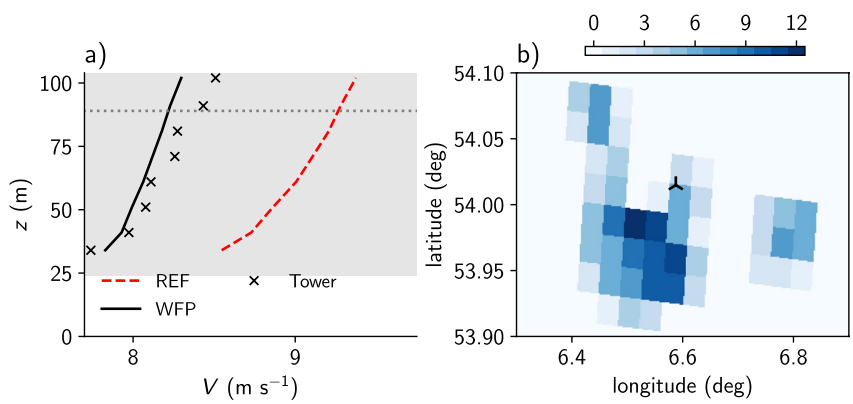

Figure 6. (a) Vertical profiles of wind speed, from the reference run without wind-farm parameterization (REF) and experiment with wind-farm parameterization (WFP), compared to the FINO1 tower. (b) The number of turbines in the HARMONIE grid cells surrounding FINO1.

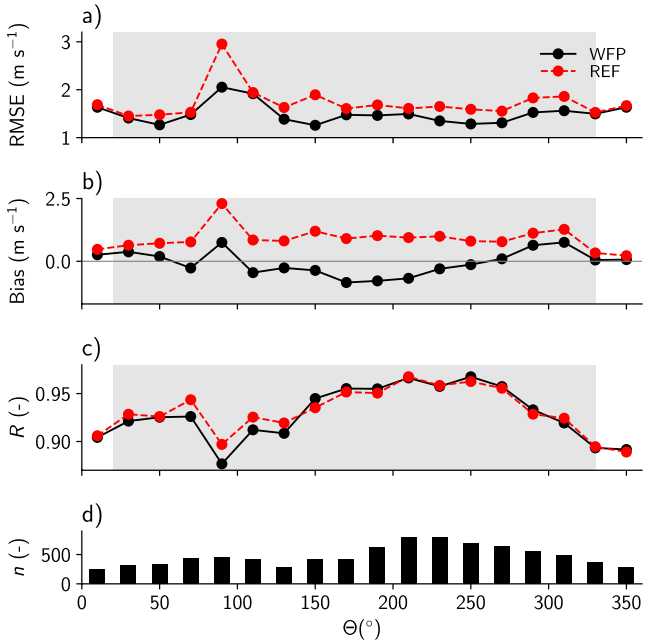

Figure 7. Verification of the wind speed at 81 m with the FINO1 tower binned per wind direction (a) root mean squared error (RMSE), (b) Mean bias, (c) Pearson correlation coefficient from the reference run without wind-farm parameterization (REF) and experiment with wind-farm parameterization (WFP), compared to the FINO1 tower. (d) The number of hours for each wind direction. The gray shading indicates the wind directions potentially disturbed by wind farms.

parameterization, which locally reduces wind speeds (Equations 6 and 7), but has very little influence on the timing of meso-scale wind patterns.

6.1.3. Westermost Rough Lidar

As shown in Figure 4, the data availability is limited to ∼14% of the January to May period, and even less at the three highest measurement heights. Therefore, the analysis here is limited to the lowest 214 m.

Figure 8 shows the time averaged vertical profiles of the lidar measurements and HARMONIE experiments. As with the FINO1 and Borssele locations, the reference run overestimates the wind speed. The experiment with wind turbines (WFP) is very close to the averaged lidar observations, especially near hub height. Above the rotor tips the gradient at which the wind speed increases is underestimated in the model. This results in a bias at 214 m of 0.2 m s^{-1} for the REF experiment and 0.3 m s^{-1} for the WFP experiment. Since the REF experiment also underestimates the wind speed above the rotor tip, this bias could be caused by an underestimation of the background wind speed or a measured acceleration of the wind above the rotor tip not captured by HARMONIE with the WFP. In order to analyse this, we would suggest experiments with higher vertical resolutions and evaluate the representation of the maritime boundary layer in this area.

6.2. Airbourne Measurements

For the evaluation of HARMONIE with the wind-farm parameterization the lidar and tower measurements show significant improvements at single locations. However, in order to evaluate the spatial scale of the modeled wakes airbourne measurements are used. The WIPAFF measurement flights are intended to observe the spatial extent of the wind-farm wakes. As mentioned in sect. 5.4, we only use the airbourne measurements carried out during 6 September 2016, with a near-neutral – slightly stable surface layer and an average wind speed of 7 m s^{-1} around hub height (Lampert et al., 2020). In those cases we expect to see a large wake from the wind farm, but not as strong as in very stable conditions (e.g., Zhan et al., 2020). Figure 9 compares the flight measurements with the HARMONIE simulations following the same track. For each measurement point the nearest model point in time and space was extracted for both REF and WFP simulations. The model output was linearly interpolated between the nearest two model levels to 90 m, the flying altitude. The wind speed from the REF simulation is shown to indicate the spatial variability of the background wind field and to differentiate the model's representation of the background wind field compared to the influence of the wind farms.

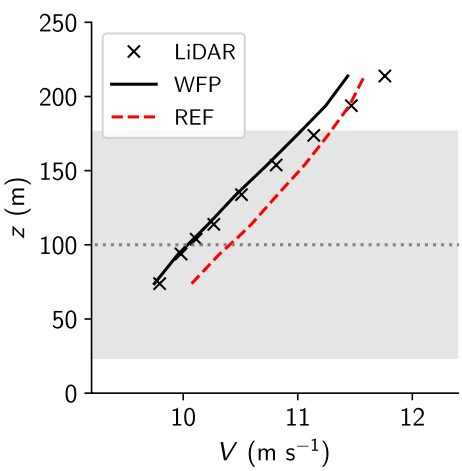

Figure 8. Vertical profiles of wind speed, from the reference run without wind-farm parameterization (REF) and experiment with wind-farm parameterization (WFP), compared to the Westermost rough lidar.

Close to the wind farm the wind farm wake is captured very well by the WFP (Figure 9a). Here, at ∼4 km distance the velocity deficit is about 2 m s^{-1} and the width of the wind farm is about 15 km. During this time the background wind speed decreases left to right of the wind farm (negative to positive $x - \overline{x_{\text{turbines}}}$), however this is underestimated by the model leading to a bias of 1.0 m s^{-1} in the WFP run. An 1.5 hr later (∼14:30) a cross section was taken at about 7.3 km downwind of the wind farm (Figure 9b). Here, the HARMONIE WFP run is able to capture the wind speed in the wake of the turbines very well, but now underestimates the wind speed east of the turbines (positive $x - \overline{x_{\text{turbines}}}$)) by about 0.7 m s^{-1}. About 10 km downwind of the previous cross section (Figure 9c), the velocity deficit in the wind-farm wake has been reduced to ∼1 m s^{-1}, captured well by in the WFP run. As expected, the REF run is unable to model the velocity deficit caused by the wind farm.

The part of the flight along the wind direction captures the recovery of the wake (Figure 9d). About 4 km away from the wind farm the wind speed is

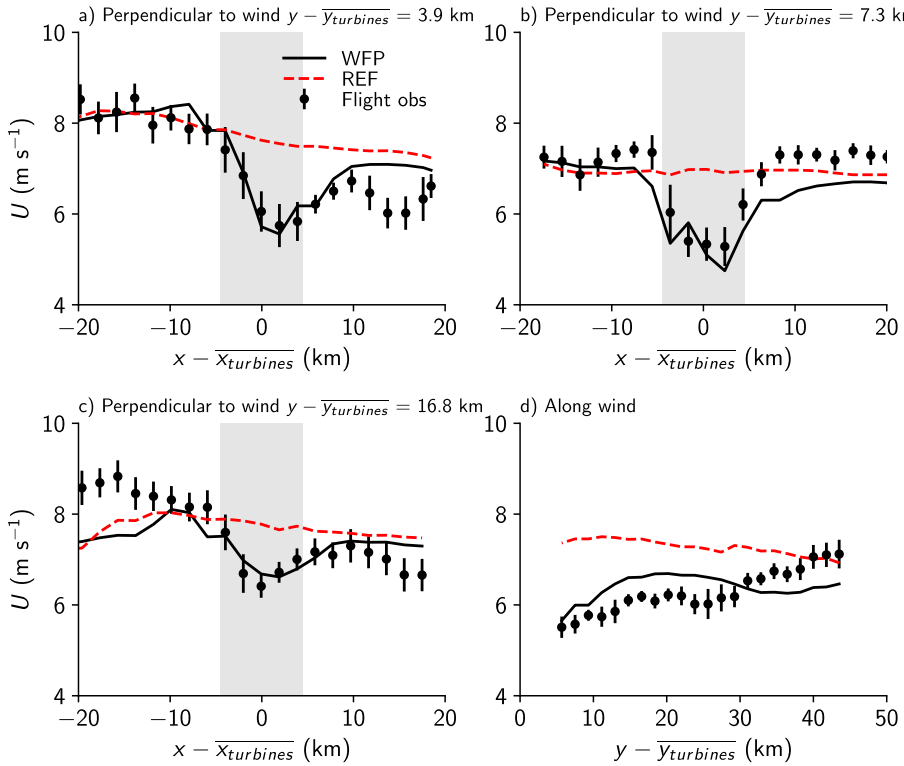

Figure 9. Cross sections through the wind farm wake of Amrumbank West in the German Bight on 6 September 2016, 12:13–15:20 UTC. Cross sections are perpendicular to the wind direction at (a) 3.9 km, (33 times the rotor diameter) (b) 7.3 km (61 times the rotor diameter), and (c) 16.8 km (140 times the rotor diameter) distance from the turbines, and (d) a cross section along the wind from the center of the turbines directly downstream. Dots indicate 60 s rolling average wind speeds at 30 s intervals, and the error bars the standard deviation from the aircraft measurements and lines indicate the interpolated modeled wind speed along the same flight path (red) reference run and (black) simulation with WFP. The gray are indicate the location of the wind farm.

5.4 m s^{-1}, at 30 km away the wind speed has only increased by 0.7 m s^{-1} to 6.1 m s^{-1}. Over the same distance the model shows a similar reduction in the velocity deficit, 0.8 m s^{-1}. After 30 km the observations show the wake to dissipate quickly, while in HARMONIE there remains a difference between the REF and WFP runs of about <0.5 m s^{-1} for at least 70 km downwind of the wind farm. The Fitch et al. (2012) parameterization is known to produce long wakes (e.g., Shepherd et al., 2020). However, a more systematic evaluation of the size and shape of wakes using Fitch et al. (2012) is needed, with more research aircraft data, scanning doppler lidars (e.g., Banta et al., 2015; Rhodes & Lundquist, 2013; Santoni et al., 2020; Schneemann et al., 2020), or satellite measurements such as SAR (e.g., Christiansen & Hasager, 2005; Hasager et al., 2015).

6.3. Power Production

When evaluating HARMONIE with the wind-farm parameterization, power production is a crucial quantity. Power production scales with the velocity cubed (Equation 9), making it sensitive to biases in wind speed. For the entire year 2016, Elia provides power production data for the Belgian offshore wind farms. This is the total power production of all the offshore wind farms. In 2016 these farms had a total capacity of 712.2 MW (Figure 3).

Figure 10 shows the comparison between the observed power production and power production obtained from the HARMONIE experiments, both from the reference experiment and experiment with the wind turbine parameterization (WFP). The bottom panels indicate the absolute and relative differences, averaged over 50 MW bins. The relative bias from the first (0–50 MW) bin should be treated with caution, as conditions where the observed power production equals zero result in an infinitely large relative bias.

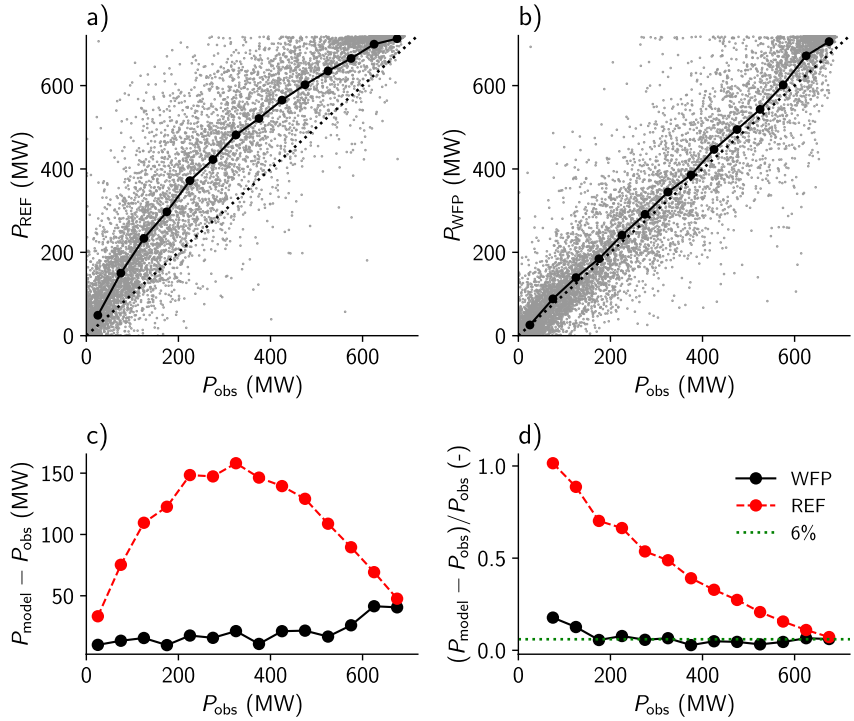

Figure 10. Power production calculated from the (a) reference reanalysis (REF) and (b) experiment with wind-farm parameterization (WFP), compared to the Elia measurements. The solid black line with markers (top row) indicates the mean of the model data calculated over 50 MW bins. The bottom row shows the (c) absolute and (d) relative error of both model experiments.

In the WFP experiment, the power production is calculated online in HARMONIE using Equation 9. The procedure is fairly straightforward: for each wind turbine, the absolute wind speed is linearly interpolated in height from the native model grid to hub height, and Equation 9 is used to calculate the power production, which is summed over all turbines in a grid point. For the reference experiment, the exact same procedure is applied offline using the three dimensional velocity fields on the native model grid, using the same amount, location, and properties (C_P curves).

The power production calculated offline from the reference experiment clearly overestimates the production, with absolute biases as large as 150 MW, and for low wind speeds (low power production) relative biases as large as 100%. The reference simulation clearly does not include the power production losses attributed to the velocity deficit created by the wind turbines. Including the wind turbine parameterization clearly improves the power production calculated, reducing the absolute bias to a maximum of 50 MW at high wind speeds, and the relative bias to ~6%. There are a few possible causes for this constant relative bias—For example, efficiency losses in the turbines or power cables, the use of (manufacturers) turbine specifications which are too optimistic, inaccuracies in the turbine parameterization, or single turbines that are not operational, or not functioning optimally. If the aim is to deliver power production forecasts to users, some post processing will be necessary to eliminate these inaccuracies.

6.4. Impact of Wind Farms on Local Meteorological Conditions

As seen in the previous sections, wind turbines have an impact on the (local) wind conditions. In addition, wind turbines generate TKE, which enhances vertical mixing, potentially influencing other quantities like temperature, humidity, or clouds. Here, we briefly examine the impact of two Dutch offshore wind farms on the local meteorological conditions. In the absence of suitable measurements, the results are limited to comparing the reference simulations with the experiment including wind turbines. As previous studies suggest an impact of atmospheric stability on wake structures (e.g., Dörenkämper et al., 2015), we have split up the data for stable and unstable lower atmospheric conditions. The bulk Richardson number (Ri_B) is calculated locally as follows:

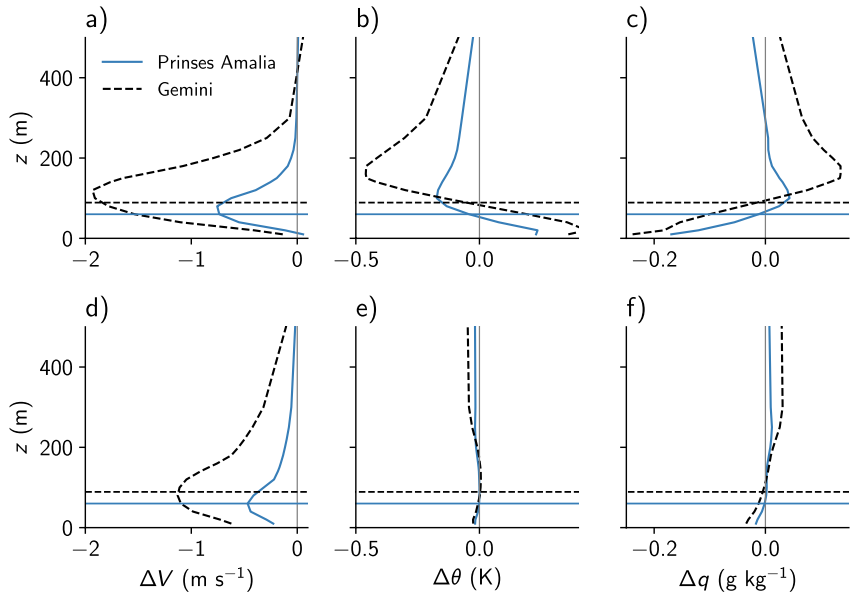

Figure 11. (a and d) Impact of wind turbines on meteorological variables wind velocity, (b and e) potential temperature, and (c and f) specific humidity over two Dutch offshore wind farms, Gemini to the north of the Dutch coast (black dashed) and Princes Amalia to the west of the Dutch coast (blue solid), where Δ = WFP-REF. The top panels (a–c) are averaged profiles where the local bulk Richardson number (Ri_B) (between 10 and 150 m) $Ri_B > 0.2$, the bottom panels (number of hours: $N_{\text{Pr.Amalia}} = 2282$ and $N_{\text{Gemini}} = 1988$) (d–f) the $Ri_B < -0.2$ (number of hours: $N_{\text{Pr.Amalia}} = 4847$ and $N_{\text{Gemini}} = 5146$). The horizontal lines indicate the hub height of each wind farm.

$$Ri_B = \frac{g}{\theta_v} \frac{\frac{\Delta\theta_v}{\Delta z}}{\left(\frac{\Delta u}{\Delta z}\right)^2 + \left(\frac{\Delta v}{\Delta z}\right)^2} \tag{10}$$

where g is the gravitational constant (=9.81 m s^{-2}), and θ_v the virtual potential temperature. Ri_B is calculated using the reference simulation at the location of the two wind farms between a height of 10 and 150 m, as this covers the entire wind turbine height for both wind farms.

Stable situations are defined as $Ri_B > 0.2$ and unstable situations as $Ri_B < -0.2$. Stable bulk Richardson numbers are more likely to occur during March – June, as the sea surface temperature is colder on average compared to the atmospheric temperature. Most unstable marine boundary layers in this area occur between September and December, when the sea surface is generally warmer than the atmosphere above. The number of hours for each stability class per month is shown in the supplementary information.

Figure 11 shows the differences in wind speed (V), potential temperature (θ), and specific humidity (q) between the experiments with and without wind turbines averaged for stable and unstable boundary layers. For wind speed, the elevated drag is clearly visible, with a maximum decrease of 1.9 m s^{-1} near hub height, but a near-surface decrease of 0.3–0.0 m s^{-1}. The relatively small wind farm Princes Amalia (120 MW, −0.75 m s^{-1} during stable and −0.4 m s^{-1} in unstable conditions) has a smaller impact on the wind speed compared to the larger Gemini (600 MW, −1.9 m s^{-1} during stable and −1.1 m s^{-1} in unstable conditions). As shown in previous research (e.g., Dörenkämper et al., 2015), we see higher velocity deficits during stable cases compared to unstable atmospheric boundary layers. In addition, stable conditions also show the wake is spread out over a shallower layer, compared to unstable conditions. During unstable conditions, the boundary layer is generally deeper, and the velocity deficit is spread out over a larger layer more than five times the hub height.

The enhanced vertical mixing has some impact on temperature and specific humidity. For stably stratified conditions, the enhanced TKE and vertical mixing decreases the stratification, resulting in an increase in temperature and decrease in specific humidity near the surface, and decrease in temperature and increase in specific humidity at 100–150 m height. At the large wind farm, Gemini, this average vertical potential temperature variation is

between −0.46 and 0.41 K, for the smaller wind farm (Princes Amalia) −0.18 to 0.23 K. The specific humidity during spring decreases by 0.24 g kg^{-1} for Gemini and 0.17 g kg^{-1} for Princes Amalia near the surface and increases by 0.13 and 0.04 g kg^{-1}, respectively, above hub height. These results are similar to those seen using WRF (Siedersleben, Lundquist, et al., 2018). As a result of the near surface heating and drying, and the cooling and moistening aloft, the relative humidity decreases near the surface, and increases higher up. This could impact the formation of fog or low clouds.

During unstable conditions the influence of the enhanced vertical mixing by wind turbines is smaller, for potential temperature less than 0.05 K and specific humidity less than 0.04 g kg^{-1} for both wind farms. The already well-mixed profiles during unstable conditions are barely influenced by enhanced TKE.

7. Conclusion

The Fitch et al. (2012) wind-farm parameterization was implemented in mesoscale model HARMONIE-AROME, and validated with a variety of observations in the north-sea region over a 1-year period. The parameterization reduces momentum and converts this into turbulent kinetic energy and power production, depending on wind turbine properties. Two one-year-long simulations were performed, one including all wind turbines on the North Sea known up to 2016 and one without any wind turbines. The evaluation with various wind measurements on the North Sea indicates that inclusion of the turbine parameterization has a positive impact on the modeled wind speeds near (offshore) wind farms. For all locations considered, the absolute bias in wind speed is decreased compared to the simulation without wind farms. Furthermore, the predicted power production—Compared to observations from the Belgian TSO—Shows a substantial improvement with the turbine parameterization included.

A brief survey of the impact of wind farms on the local meteorological conditions, indicates that in addition to changes in wind speed, other quantities like temperature or humidity are influenced by wind farms as well. These variations in temperature and humidity are more pronounced in periods with more stable conditions, where the enhanced turbulent kinetic energy from the wind turbines increases the mixing of the marine boundary layer. With the expected increase in number and size of wind turbines in the coming decades the influence of wind turbines on local to regional meteorology can no longer be neglected. The relatively simple wind-farm parameterization by Fitch et al. (2012) improves modeled wind speed near wind farms and can be used operationally to improve weather forecasts and predicted power production.

Data Availability Statement

The input data for the wind farm parameterisation together with the HARMONIE-AROME output used to make all figures is available at: https://doi.org/10.5281/zenodo.6427317. The measurements used in the manuscript have various sources. Borssele wind farm zone lidars: https://offshorewind.rvo.nl/cms/view/78f1a154-5b56-4ab0-a70f-d746a610179e/studies-borssele, FINO1 tower data: https://www.fino1.de/en/, Westermost Rough wind farm zone lidar: https://orsted.com/en/our-business/offshore-wind/wind-data, WIPAFF flight measurements: https://doi.pangaea.de/10.1594/PANGAEA.902845, and Elia power production data: https://opendata.elia.be/ The HARMONIE-AROME reference simulations are available on the KNMI data platform: https://data-platform.knmi.nl/dataset/?tags=Dutch+Offshore+Wind+Atlas. Access to the HARMONIE-AROME codes can be obtained by contacting one of the member institutes of the HIRLAM consortium and is subject to signing a standardised ALADIN-HIRLAM licence agreement (see http://www.hirlam.org/). and other contributors.

Acknowledgments
The authors would like to acknowledge funding from the Dutch Offshore Wind Atlas (DOWA) project supported with Topsector Energy subsidy from the Ministry of Economic Affairs and Climate Policy, and the Topconsortia for Knowledge and Innovation (TKI) funded Winds of the North Sea in 2050 (WINS50) project. The authors would like to thank ECMWF for providing computational resources. We would also like to thank Jeanette Onvlee, Sukanta Basu, and Pier Siebesma for fruitfull discussions.

References

Abkar, M., & Porté-Agel, F. (2015). A new wind-farm parameterization for large-scale atmospheric models. *Journal of Renewable and Sustainable Energy*, *7*(1), 013121. https://doi.org/10.1063/1.4907600

Acker, T., & Chime, A. H. (2011). *Wind modeling using WindPro and WAsP software*. Norther Arizon University. 510.

Archer, C. L., Wu, S., Ma, Y., & Jiménez, P. A. (2020). Two corrections for turbulent kinetic energy generated by wind farms in the WRF model. *Monthly Weather Review*, *148*(12), 4823–4835. https://doi.org/10.1175/mwr-d-20-0097.1

Baidya Roy, S., & Traiteur, J. J. (2010). Impacts of wind farms on surface air temperatures. *Proceedings of the National Academy of Sciences*, *107*(42), 17899–17904. https://doi.org/10.1073/pnas.1000493107

Banta, R. M., Pichugina, Y. L., Brewer, W. A., Lundquist, J. K., Kelley, N. D., Sandberg, S. P., et al. (2015). 3D volumetric analysis of wind turbine wake properties in the atmosphere using high-resolution Doppler lidar. *Journal of Atmospheric and Oceanic Technology*, *32*(5), 904–914.

Bärfuss, K., Hankers, R., Bitter, M., Feuerle, T., Schulz, H., Rausch, T., et al. (2019). In-situ airborne measurements of atmospheric and sea surface parameters related to offshore wind parks in the German Bight. PANGAEA https://doi.org/10.1594/PANGAEA

Bengtsson, L., Andrae, U., Aspelien, T., Batrak, Y., Calvo, J., de Rooy, W., et al. (2017). The HARMONIE–AROME model configuration in the ALADIN–HIRLAM NWP system. *Monthly Weather Review*, *145*(5), 1919–1935. https://doi.org/10.1175/mwr-d-16-0417.1

Christiansen, M. B., & Hasager, C. B. (2005). Wake effects of large offshore wind farms identified from satellite SAR. *Remote Sensing of Environment*, *98*(2–3), 251–268. https://doi.org/10.1016/j.rse.2005.07.009

Davies, H. (1976). A lateral boundary formulation for multi-level prediction models. *Quarterly Journal of the Royal Meteorological Society*, *102*(432), 405–418. https://doi.org/10.1256/smsqj.43209

de Haan, S. (2011). High-resolution wind and temperature observations from aircraft tracked by Mode-S air traffic control radar. *Journal of Geophysical Research*, *116*(D10). https://doi.org/10.1029/2010jd015264

de Haan, S. (2016). Estimates of Mode-S EHS aircraft-derived wind observation errors using triple collocation. *Atmospheric Measurement Techniques*, *9*(8), 4141–4150. https://doi.org/10.5194/amt-9-4141-2016

de Rooy, W. C., Siebesma, P., Baas, P., Lenderink, G., de Roode, S., de Vries, H., et al. (2022). Model development in practice: A comprehensive update to the boundary layer schemes in HARMONIE-AROME. *Geoscientific Model Development*, *15*(4), 1513–1543. https://doi.org/10.5194/gmd-15-1513-2022

Dörenkämper, M., Witha, B., Steinfeld, G., Heinemann, D., & Kühn, M. (2015). The impact of stable atmospheric boundary layers on wind-turbine wakes within offshore wind farms. *Journal of Wind Engineering and Industrial Aerodynamics*, *144*, 146–153. https://doi.org/10.1016/j.jweia.2014.12.011

Duncan, J. B., Wijnant, I. L., & Knoop, S. (2019). DOWA validation against offshore mast and LiDAR measurements. *Tech. Rep. No. TNO technical report 2019 R10062*. Retrieved from https://www.dutchoffshorewindatlas.nl/publications/reports/2019/05/21/tno-report-dowa-validation-against-offshore-mast-and-lidar-measurements

Faroux, S., Kaptué Tchuenté, A., Roujean, J.-L., Masson, V., Martin, E., & Moigne, P. L. (2013). ECOCLIMAP-II/Europe: A twofold database of ecosystems and surface parameters at 1 km resolution based on satellite information for use in land surface, meteorological and climate models. *Geoscientific Model Development*, *6*(2), 563–582. https://doi.org/10.5194/gmd-6-563-2013

Fischer, C., Montmerle, T., Berre, L., Auger, L., & Ştefănescu, S. E. (2005). An overview of the variational assimilation in the ALADIN/France numerical weather-prediction system. *Quarterly Journal of the Royal Meteorological Society*, *131*(613), 3477–3492. https://doi.org/10.1256/qj.05.115

Fischereit, J., Brown, R., Larsén, X. G., Badger, J., & Hawkes, G. (2021). Review of mesoscale wind-farm parametrizations and their applications. *Boundary-Layer Meteorology*, 1–50. https://doi.org/10.1007/s10546-021-00652-y

Fitch, A. C., Olson, J. B., Lundquist, J. K., Dudhia, J., Gupta, A. K., Michalakes, J., & Barstad, I. (2012). Local and mesoscale impacts of wind farms as parameterized in a mesoscale NWP model. *Monthly Weather Review*, *140*(9), 3017–3038. https://doi.org/10.1175/mwr-d-11-00352.1

Gustafsson, N., Janjić, T., Schraff, C., Leuenberger, D., Weissmann, M., Reich, H., et al. (2018). Survey of data assimilation methods for convective-scale numerical weather prediction at operational centres. *Quarterly Journal of the Royal Meteorological Society*, *144*(713), 1218–1256. https://doi.org/10.1002/qj.3179

Hasager, C. B., Vincent, P., Badger, J., Badger, M., Di Bella, A., Peña, A., et al. (2015). Using satellite SAR to characterize the wind flow around offshore wind farms. *Energies*, *8*(6), 5413–5439. https://doi.org/10.3390/en8065413

Hersbach, H., Bell, B., Berrisford, P., Hirahara, S., Horányi, A., Muñoz-Sabater, J., et al. (2020). The ERA5 global reanalysis. *Quarterly Journal of the Royal Meteorological Society*, *146*(730), 1999–2049. https://doi.org/10.1002/qj.3803

Lampert, A., Bärfuss, K., Platis, A., Siedersleben, S., Djath, B., Cañadillas, B., et al. (2020). In situ airborne measurements of atmospheric and sea surface parameters related to offshore wind parks in the German Bight. *Earth System Science Data*, *12*(2), 935–946. https://doi.org/10.5194/essd-12-935-2020

Lee, J. C., & Lundquist, J. K. (2017). Evaluation of the wind farm parameterization in the Weather Research and Forecasting model (version 3.8.1) with meteorological and turbine power data. *Geoscientific Model Development*, *10*(11), 4229–4244. https://doi.org/10.5194/gmd-10-4229-2017

Lenderink, G., & Holtslag, A. A. (2004). An updated length-scale formulation for turbulent mixing in clear and cloudy boundary layers. *Quarterly Journal of the Royal Meteorological Society: A journal of the atmospheric sciences, applied meteorology and physical oceanography*, *130*(604), 3405–3427. https://doi.org/10.1256/qj.03.117

Marseille, G.-J., & Stoffelen, A. (2017). Toward scatterometer winds assimilation in the mesoscale HARMONIE model. *IEEE Journal of Selected Topics in Applied Earth Observations and Remote Sensing*, *10*(5), 2383–2393. https://doi.org/10.1109/jstars.2016.2640339

Martín Míguez, B., Novellino, A., Vinci, M., Claus, S., Calewaert, J.-B., Vallius, H., et al. (2019). The European marine observation and data Network (EMODnet): Visions and roles of the gateway to marine data in Europe. *Frontiers in Marine Science*, *6*, 313. https://doi.org/10.3389/fmars.2019.00313

Masson, V., Le Moigne, P., Martin, E., Faroux, S., Alias, A., Alkama, R., et al. (2013). The SURFEXv7.2 land and ocean surface platform for coupled or offline simulation of Earth surface variables and fluxes. *Geoscientific Model Development*, *6*(4), 929–960. https://doi.org/10.5194/gmd-6-929-2013

Muñoz-Esparza, D., Cañadillas, B., Neumann, T., & Van Beeck, J. (2012). Turbulent fluxes, stability and shear in the offshore environment: Mesoscale modelling and field observations at FINO1. *Journal of Renewable and Sustainable Energy*, *4*(6), 063136. https://doi.org/10.1063/1.4769201

Platis, A., Bange, J., Bärfuss, K., Cañadillas, B., Hundhausen, M., Djath, B., et al. (2020). Long-range modifications of the wind field by offshore wind parks–results of the project WIPAFF. *Meteorologische Zeitschrift*, 355–376. https://doi.org/10.1127/metz/2020/1023

Platis, A., Hundhausen, M., Mauz, M., Siedersleben, S., Lampert, A., Bärfuss, K., et al. (2021). Evaluation of a simple analytical model for offshore wind farm wake recovery by in situ data and weather research and forecasting simulations. *Wind Energy*, *24*(3), 212–228. https://doi.org/10.1002/we.2568

Rhodes, M. E., & Lundquist, J. K. (2013). The effect of wind-turbine wakes on summertime us midwest atmospheric wind profiles as observed with ground-based Doppler lidar. *Boundary-Layer Meteorology*, *149*(1), 85–103. https://doi.org/10.1007/s10546-013-9834-x

Santoni, C., García-Cartagena, E. J., Ciri, U., Zhan, L., Valerio Iungo, G., & Leonardi, S. (2020). One-way mesoscale-microscale coupling for simulating a wind farm in North Texas: Assessment against SCADA and LiDAR data. *Wind Energy*, *23*(3), 691–710. https://doi.org/10.1002/we.2452

Schneemann, J., Rott, A., Dörenkämper, M., Steinfeld, G., & Kühn, M. (2020). Cluster wakes impact on a far-distant offshore wind farm's power. *Wind Energy Science*, *5*(1), 29–49. https://doi.org/10.5194/wes-5-29-2020

Shepherd, T., Barthelmie, R., & Pryor, S. (2020). Sensitivity of wind turbine array downstream effects to the parameterization used in WRF. *Journal of Applied Meteorology and Climatology*, *59*(3), 333–361.

Siedersleben, S. K., Lundquist, J. K., Platis, A., Bange, J., Bärfuss, K., Lampert, A., et al. (2018). Micrometeorological impacts of offshore wind farms as seen in observations and simulations. *Environmental Research Letters*, *13*(12), 124012. https://doi.org/10.1088/1748-9326/aaea0b

Siedersleben, S. K., Platis, A., Lundquist, J. K., Djath, B., Lampert, A., Bärfuss, K., et al. (2020). Observed and simulated turbulent kinetic energy (WRF 3.8.1) overlarge offshore wind farms. *Geoscientific Model Development*.

Siedersleben, S. K., Platis, A., Lundquist, J. K., Lampert, A., Bärfuss, K., Cañadillas, B., et al. (2018). Evaluation of a wind farm parametrization for mesoscale atmospheric flow models with aircraft measurements. *Meteorologische Zeitschrift (Berlin)*, *27*, NREL/JA-5000-73670). https://doi.org/10.1127/metz/2018/0900

Skamarock, W. C., Klemp, J. B., Dudhia, J., Gill, D. O., Liu, Z., Berner, J., et al. (2019). *A description of the advanced research WRF model version 4* (Vol. 145). National Center for Atmospheric Research.

Volker, P., Badger, J., Hahmann, A. N., & Ott, S. (2015). The explicit wake parametrisation V1. 0: A wind farm parametrisation in the mesoscale model WRF. *Geoscientific Model Development*, *8*(11), 3715–3731.

Wagner, D., Steinfeld, G., Witha, B., Wurps, H., & Reuder, J. (2019). Low level jets over the southern North Sea. *Meteorologische Zeitschrift*, 389–415. https://doi.org/10.1127/metz/2019/0948

Westerhellweg, A., Canadillas, B., Beeken, A., & Neumann, T. (2010). One year of LiDAR measurements at FINO1-Platform: Comparison and verification to met-mast data. In *Proceedings of 10th german wind energy conference dewek* (pp. 1–5).

Westerhellweg, A., Neumann, T., & Riedel, V. (2012). *FINO1 mast correction* (Vol. 21). DEWI-Magazin.

Wijnant, I. L., van Ulft, B., van Stratum, B. J. H., Barkmeijer, J., Onvlee, J., de Valk, S., et al. (2019). The Dutch offshore wind atlas (DOWA): description of the dataset (Tech. Rep.). Retrieved from https://www.dutchoffshorewindatlas.nl/publications

WindEurope. (2017). Wind energy in europe: Scenarios for 2030 (Tech. Rep.). Retrieved from https://windeurope.org/wp-content/uploads/files/about-wind/reports/Wind-energy-in-Europe-Scenarios-for-2030.pdf

Witkin, A. P., & Heckbert, P. S. (2005). Using particles to sample and control implicit surfaces. In *Acm siggraph 2005 courses*. https://doi.org/10.1145/1198555.1198656.260

Wu, C., Luo, K., Wang, Q., & Fan, J. (2022). A refined wind farm parameterization for the weather research and forecasting model. *Applied Energy*, *306*, 118082. https://doi.org/10.1016/j.apenergy.2021.118082

Zhan, L., Letizia, S., & Valerio Iungo, G. (2020). LiDAR measurements for an onshore wind farm: Wake variability for different incoming wind speeds and atmospheric stability regimes. *Wind Energy*, *23*(3), 501–527. https://doi.org/10.1002/we.2430